Meteorology and Atmospheric Physics
https://doi.org/10.1007/s00703-019-00682-9

ORIGINAL PAPER

Synoptic analysis and mesoscale numerical modelling of heavy precipitation: a case study of flash flood event in Kota Kinabalu, Malaysia

Jackson Hian-Wui Chang[1] · **S. S. K. Kong**[2] · **Justin Sentian**[3] · **Jedol Dayou**[4] · **Fuei-Pien Chee**[4]

Received: 22 October 2018 / Accepted: 4 July 2019

Abstract

A case of severe flash flood event affecting Kota Kinabalu (KK) on 17 Jul 2005 is analyzed by means of synoptic analysis using ERA-Interim Reanalysis and NCEP-FNL Data sets. In the synoptic scale, significant amount of precipitation was recorded in Sabah on 16 Jul and 17 Jul 2005. The heavy rainfall was associated to the upper-level ridge and lower-level cyclone observed over the South China Sea. Several low-pressure centers were also noticed over the Philippines Sea which were believed to intensify the heavy rainfall in Sabah. The vertical cross section for divergence along 116°E at Kota Kinabalu also revealed that a significant convergence was observed near the surface and accompanied by a strong updraft of divergence at upper-level. In the mesoscale, the ability of the convection-permitting WRF model to reproduce the convective cells associated with the heavy rainfall event is examined. A triply nested WRF model with the highest resolution of 5-km horizontal grid spacing was integrated with conventional analysis data. The simulation results were validated against observation from TRMM, CHIRPS, and PERSIANN-CDR. The modelled results agree moderately to the observation and fairly well simulated the initiation, intensification, and deceleration of heavy rainfall at nearly the right time except for some mismatch in terms of spatial distribution. The corresponding precipitation amount was also reasonably reproduced in its distribution but slightly overestimated. We also found that the cause of this severe flash flood is rooted to the prolonged heavy rainfall in the KK region induced by Typhoon Haitang.

1 Introduction

Flood is an overflow of water that submerges land that is usually dry. It can happen during heavy rains, when ocean waves come on shore, when snow melts too fast or when dam or levees break. The effect could be quickly over or extend a long period and may last for days, weeks or longer depending on the severity of the flood magnitude (Zhou et al. 2017). Floods are the most common and widespread of all weather-related natural disasters. Among many types of flood, flash flood is the most dangerous kind of flood because it occurs with an incredible speed and is unpredictable (Hong and Lee 2009). It usually occurs when excessive water fills the dry creeks or river beds along with flowing creeks and rivers, causing rapid rises of water within very short period of time. In the mesoscale, many simulation studies have shown that when the model runs at high resolution down to 10 km or less can reproduce the observed mesoscale features such as intense squall line (Zhang et al. 1988), winter storm over mountainous terrain (Bruintjes et al. 1994), low-level flow and precipitation over mountainous area (Colle and Mass

Responsible Editor: E.-K. Jin.

✉ Jackson Hian-Wui Chang
jacksonchw@ums.edu.my

1 Preparatory Center for Science and Technology (PPST) , Universiti Malaysia Sabah , Jalan UMS, 88400 Kota Kinabalu, Malaysia

2 Cloud and Aerosol Laboratory, Department of Atmospheric Sciences , National Central University , Taoyuan 32001, Taiwan, ROC

3 Climate Change Research Group (CCRG), Faculty of Science and Natural Resources , Universiti Malaysia, Sabah , Jalan UMS, 88400 Kota Kinabalu, Malaysia

4 Energy, Vibration and Energy Research Group (e-VIBS), Faculty of Science and Natural Resources , Universiti Malaysia, Sabah , Jalan UMS, 88400 Kota Kinabalu, Malaysia

Published online: 19 July 2019

1996), real-time precipitation forecast over mountains (Gaudet and Cotton 1998). However, systematic deficiencies in the model precipitation include varying horizontal resolution for different types of storm (Colle et al. 2000; Mass et al. 2002), different initial conditions forcing (Gallus et al. 2005), sensitivity of model to different parameterizations (Raju et al. 2011; Efstathiou et al. 2013) often cause poor representation of warm season convective system (Gallus et al. 2005). The accuracy of the model to explicitly resolve convective systems without parameterized convection lies close to the high-resolution near-surface measurements and observation for initial mechanism (Wilson and Roberts 2006), wavelike mechanisms in the free troposphere and/or the planetary boundary layer (Carbone et al. 2002) and assimilation of sites within a single database linked through space and time for mutually supportive holistic analysis (Davis et al. 2003).

The evolution of numerical weather prediction (NWP) models from software requiring extensive computational resources to standalone packages such as Weather Research Forecast (WRF) model capable of running on inexpensive desktop computers has provided the flood forecaster to predict heavy precipitation events. The WRF model can be implemented on inexpensive computers, using default parameters, and on a relatively large spatial resolution grid to provide an accessible tool for better understanding flooding events. For example, Flesch and Reuter (2012) successfully simulated two Alberta flooding events using Weather Research Forecasts (WRF) models at 25-km grid resolution. Cardoso et al. (2013) also simulated the Iberian mean and extreme precipitation event in the period 1989–2009 using the WRF model performed at two nested grids at 27-km and 9-km horizontal resolution. Based on their findings, higher resolution simulation basically indicates better representation of the precipitation fields at all timescales with emphasis on the representation of variability and of extreme weather statistics. Hong et al. (2010) also found that high-resolution dynamics and physics in the WRF model seem to be major advantages in resolving meso- to cloud resolving features in response to complex orography. For that, the increase in computer power nowadays has significantly improved the regional downscaling to less than 5-km horizontal grid resolution. It allows the explicit resolution of dynamical and thermo-dynamical processes associated with the convective, especially the related terrain features that can have direct impacts on precipitation. For example, Xue and Martin (2006) presented a high-resolution numerical simulation of the 24 May 2002 dry-line convective initiation (CI) case during the International H20 Project (IHOP) using the Advanced Regional Prediction System (ARPS) at a 3-km grid resolution. Weisman et al. (2008) reported that significant value was added for the high-resolution forecasts at 4-km grid spacing in representing the convective system mode (e.g., for squall lines, bow echoes, mesoscale convective vortices) as well as in representing the diurnal convective cycle. Song and Sohn (2018) presented a systematic simulation at 5-km resolution over the southern part of the Korean peninsula to mimic the heavy rainfall around the complex terrain features of Jirisan mountain using multiple microphysical parameterization.

In Sabah, monsoonal flood and flash flood are the two most common floods; the flood height in monsoonal flood can take up to few months to return to its normal level but only few hours for flash flood. Nevertheless, flash flood has the equal severity as it usually occurs within a very short time for no timely evacuation is allowed. In addition, it is extremely difficult to be accurately forecasted in major operational weather forecast center due to its coarse resolution that is incapable of resolving the details of the complex precipitation structures that are forced by mesoscale orography, land surface heterogeneities, and land–water contrasts (Givati et al. 2011). Therefore, accurate analysis and prediction of precipitation amounts and their spatial distribution are vital for regional- and local-scale hydrological applications to improve the flash flood forecast. This is especially essential for certain areas in Sabah that are prone to flash flood in recurrence interval and have insufficient dense network of uniformly distributed rain gauge stations (Chawla et al. 2018).

In this study, we examined the ability of the WRF model to reproduce such flash-flood heavy rainfall event occurred over the west coast part of the Sabah region on 17 Jul 2005. In the synoptic scale, the flood event is investigated using ERA-Interim Reanalysis and NCEP-FNL Data sets. In the mesoscale analysis, a convection-permitting simulation at 5-km grid resolution is conducted using the WRF model, and the accuracy of the quantitative precipitation forecasts is validated against observation data. Due to the lack of in-situ monitoring ground data, the high-resolution simulation results are assessed over the available synoptic observation data. Section 2 describes the selected case and Sect. 3 describes the gridded products used in this study. Section 4 describes the mesoscale numerical model experiment setup and design. The observation analysis in synoptic scale, modelled result and the comparison against the observation are described in Sect. 5, and the discussion and conclusion are presented in Sect. 6.

2 Description of study area and flooding events history

Sabah is located in eastern Malaysia and covers an area of about 73,000 km^2. Figure 1 shows the topography features and the rainfall distribution map of Sabah. Also shown on the figure is the domain for synoptic scale on Fig. 1a

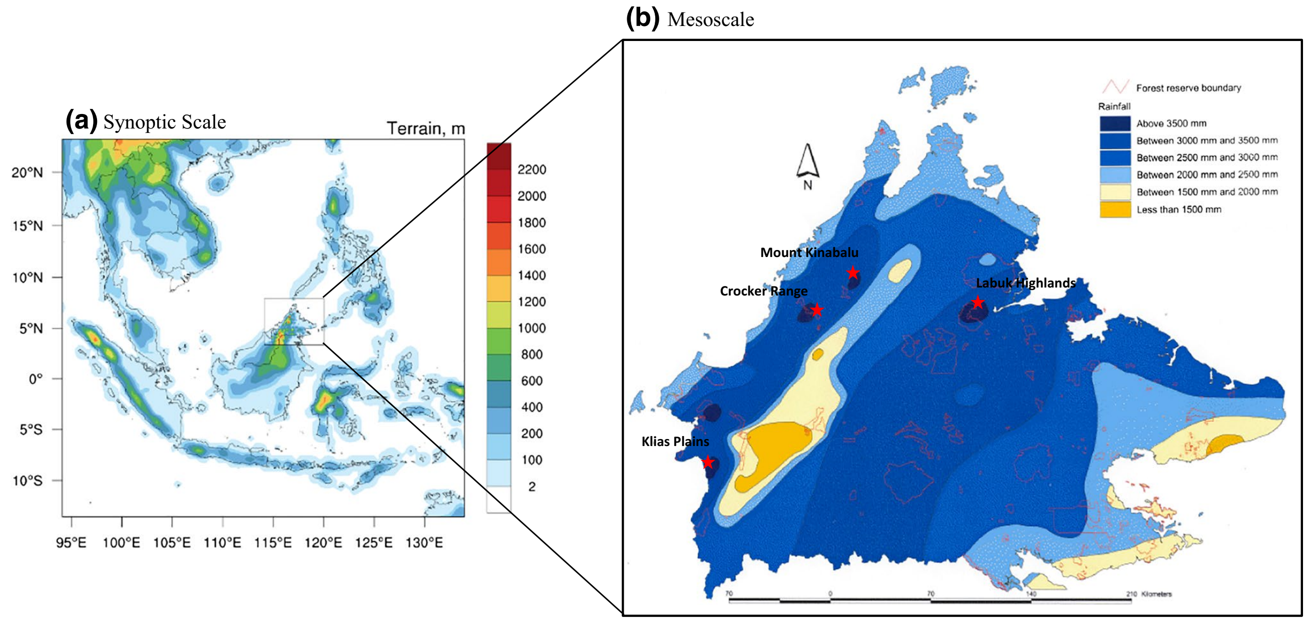

Fig. 1 Map of Southeast Asia showing the **a** topography features and **b** annual rainfall distribution map over the study area. The domain **a** and **b** also reflects the synoptic scale and mesoscale discussed in this study. [Source (b): https://www.sabah.gov.my]

and mesoscale on Fig. 1b used in this study. The priority of land use allocation has historically been mining, agriculture, forestry, and recreation/wildlife. Besides, it is also superimposed on a rather complex terrain especially over the mountainous areas around Mount Kinabalu, lies between Ranau and Kota Belud. The climate is generally categorized as warm and humid, having a narrow annual range of temperature (30–32 °C) and frequent rainfall (~2500 mm/year) throughout the year. There are two monsoon seasons: Northeast (December–March) NEM and Southwest (June–September) SWM monsoon; each separated by 2 months of inter-monsoon period. The rainy season is mainly between November and February, which is during the northeast monsoon season. On average, Sabah receives 2500–3500 mm of rainfall annually in most part of the state. Some localities obtained much lower or beyond this range due to influences of coastal and rain-shadow to large land-mass or ranges. Most of the rains are of tropical rainstorms due to ITCZ which appears as a band of clouds near the Equator driven by solar heating. It is formed by vertical motion largely appearing as convective activity of thunderstorm which effectively draw air in to form frequent tropical rainstorms. Average rainfall in 1 day can measure as much as 10 mm during NEM season, as low as 5 mm during SWM season, and 7 mm during inter-monsoon period. The highest rainfall ranges, which is above 3500 mm, estimated only to cover 1% of the state. The amount distributed on small localised windward area of Mt. Kinabalu (Komborongoh, 4095 m a.s.l.) and Crocker Range (Ulu Moyog, 2000 m), and low-lying area in south-eastern of Klias plain, and north-eastern of Labuk Highlands.

Flooding is a regular occurrence in Sabah and the severity of flooding varies from year to year. Low lying area, floodplains and developed river basin throughout Sabah experienced flood to a various extent of seriousness in terms of depth, inundated area, duration and damages. Table 1 summarizes the last few occurrences of flash-flooding events in Sabah region. On 17 Jul 2005, a severe flash-flooding event hit the Sabah region. The heavy rainfall hit the west coast of Sabah at 1400 UTC (hereinafter all timestamps are referred in UTC) causing the town, Telipok about 15 km from Kota Kinabalu to be hit by flash flood. The local news reported that the town suffered a 2 m flood height after 12-h of downpour. The floodwater began to recede at about 0200, 18 Jul. According to the flood archive by Dartmouth Flood Observatory (DFO) 2005, this event was reported as the highest water levels in 50 years in Kota Kinabalu area. The aftermath effects lasted for a total of 3 days until 19 Jul 2005 with a total of 600 residents evacuated. The severity class was raised to Class 2 indicating very large events and greater than 20 years but less than 100 years recurrence interval, and/or a local recurrence interval of at 10–20 years. The affected region extends to 1470-sq km including Kota Kinabalu area, Menggatal, Telipok, Kampung Rampaian, Kampung Tobobon and Kampung Giling. The flood magnitude was estimated to reach 3.8. Flood magnitude is a composite score of flood severity developed by DFO that encompasses severity level, recurrence interval, duration of the flood in days and the area affected. The magnitude of

Table 1 Specific flood events in Sabah and damages caused by flood. [nd: no data]

Event	Area	Causes	Damages/severity	Flood magnitude	Affected area (km^2)
24–27 Dec 1996	Borneo: Sabah state	Heavy rainfall by Tropical Storm "Greg"	170 killed 100 missing 3000 people homeless 300 homes damage	5.3	73,240
5–7 Jan 1999	Moyog	Heavy and long duration of rainfall by Tropical storm "Hilda"	5 killed 1106 evacuated 5 villages inundated 2.0–4.0 m flood height	nd	nd
4–7 Dec 2001	Membakut	Heavy rainfall	6000 evacuated 4 villages inundated 1.0 m flood height	3.5	745
17–19 Jul 2005 (study event)	Kota Kinabalu, Telipok	Torrential rainfall	3 killed 600 evacuated 2793 families affected 6 villages inundated 2.0 m flood height	3.8	1470

"0" is the smallest value (no flooding) and "10" is the largest value based on the DFO flood record (1998–present). A value of 3.8 indicates that the flood runoff volume is 0.38 to that of the flood of record (the measured current flooding/flood of record ratio multiplied by 10). The main cause of the flood was reported as brief torrential rain.

3 Gridded product

In this study, we selected three products including TRMM (satellite gridded), PERSIANN-CDR (satellite-derived gridded) and CHIRPS (satellite and station-derived gridded) to validate the modelled results and two gridded products including ERA-Interim and FNL for the synoptic analysis. Table 2 shows the summary of all the gridded products used in this study. TRMM rain rate data are available at a temporal resolution of 3 h with spatial resolution of 0.25° × 0.25° latitude–longitude grid. In this work, the real-time version (3B42RT) was used and is further termed as TRMM. The TRMM is available between 50°N and 50°S (Huffman et al. 2010). It combines the product of Infrared (IR) from geosynchronous satellite and Passive-Micro-Wave (PMW) from low orbit satellite to detect cloud top temperature and observe cloud size and cloud phase (Rahmawati and Lubczynski 2018). PERSIANN-CDR-gridded rainfall is generated

Table 2 Summary of all gridded products used in the current study

Datasets	Full name	Latitudinal coverage	Spatial resolution	Temporal coverage	Temporal resolution	References
TRMM-3B42RT	TRMM Multi-satellite Precipitation Algorithm Version 7	50°N–50°S	0.25°	Dec 1997–present	3-h	Huffman (1997) and Huffman et al (2010)
PERSIANN-CDR	PERSIANN Climate Data Record, Version 1 Revision 1	60°N–60°S	0.25°	Jan 1983–present	Daily	Sorooshian et al. (2014) and Ashouri et al. (2015)
CHIRPS	Climate Hazards group Infrared Precipitation with Stations Version 2.0	50°N–50°S	0.05°	Jan 1981–present	Daily	Funk et al. (2005)
ERA-Interim	ECMWF Re-Analysis Interim	90°N–90°S	0.75°	Jan 1989–present	6-h	Berrisford et al. (2011) and Dee el al. (2011)
FNL	NCEP FNL Operational Model Global Tropospheric Analyses ds083.2	90°N–90°S	1.00°	Jul 1997–present	6 h	Parrish and Derver (1992)

every 3 h at 0.25 × 0.25° lat/lon between 60°N and 60°S. It estimates rainfall using artificial neural network model of IR brightness temperature every 30 min provided by PMW (Hsu et al. 1997). The model uses the archive of the Gridded Satellite brightness temperature observations (GridSat-B1) of the International Satellite Cloud Climatology Project (ISCCP) to extract cold-cloud pixels and neighbouring features to estimate surface rainfall rate (Ashouri et al. 2018). CHIRPS is a quasi-global rainfall data set spanning 50°S–50°N and all longitudes. It incorporates 0.05° × 0.05° resolution satellite imagery with in-situ station data to create gridded rainfall time series data. It uses a smart interpolation approach working with anomalies from a high-resolution climatology (Funk et al. 2005).

ERA-Interim is the latest global atmospheric reanalysis produced by the European Centre for Medium-Range Weather Forecasts (ECMWF). The ERA-Interim atmospheric model and reanalysis system uses cycle 31r2 of ECMWF's Integrated Forecast System (IFS), which was configured for (1) 60 levels in the vertical, with the top level at 0.1 hPa; (2) T255 spherical-harmonic representation for the basic dynamical fields; (3) a reduced Gaussian grid with approximately uniform 79 km spacing for surface and other grid-point fields (Berrisford et al. 2011). NCEP FNL (Final) Operational Global Analysis data are on 1-degree-by-1-degree grids prepared operationally every 6 h. It is a near-real-time reanalysis product from real-time operational Global Forecast System (GFS) that is assimilated with Global Data Assimilation System (GDAS), which continuously collects observational data from the Global Telecommunications System (GTS). The analyses are available on the surface, at 26 mandatory pressure levels from 1000 to 10 mb, in the surface boundary layer and at some sigma layers, the tropopause and a few others.

4 Synoptic-observational analysis

Figure 2 shows the evolution of the rainfall intensity at an interval of 3-h accumulated precipitation from 16–17 Jul 2005 obtained from ERA-Interim Reanalysis Data sets. The spatial resolution of the data set is approximately 80 km (T255 spectral) on 60 vertical levels from the surface up to 0.1 hPa. A significant amount of precipitation was recorded in Sabah on both days particularly over the west coast division near the South China Sea. To further visualize the evolution of the rainfall, we extracted the value of rainfall at the grid points nearest to KK and plot it as a time series (see Fig. 2b). The initiation of the rainfall started at 1200 UTC 16 Jul, and continued to intensify and reached to its peak at 2100 UTC 16 Jul for about 15.0 mm. Another peak was then observed at 0900 UTC 17 Jul with a total precipitation amount of 11.0 m. The deceleration of the rainfall began at 1200 UTC 17 Jul and rainfall amount remained low until 1800 UTC. In general, the gridded precipitation pattern agrees well with the actual occurrence of the flash flood; the local news reported that the rainfall started at around 1400 UTC 17 Jul 2005, which was represented by a dotted red line on Fig. 2b, and long hours of rainfall hit the city and caused the flash flood at around afternoon–evening hours on 17 Jul 2005.

Figure 3 shows the surface weather charts analyzed by the surface and MWSL (maximum wind speed level)-analysis, obtained from the NCEP FNL. The data set has a resolution of 1° × 1°. The MWSL geopotential height field shows a remarkable high pressure over the central of South China Sea and its eastward extension to the Philippines Sea near 130°E during the heavy rainfall events from 17 to 19 Jul 2005 (Fig. 3). At 0000 UTC 16 Jul, substantial low geopotential fields were observable over the north of Philippines Sea and it extensively becomes lower on 17 Jul, and persisted until 19 Jul. At 0000 UTC 20 Jul, the geopotential fields resumed to normal as 15 Jul 2005. The extension of such pressure variation can be explained by the propagation of Rossby wave (Efstathiou et al. 2013). It is well known that there are free Rossby waves in South China Sea. The propagation of Rossby wave transmits the signal of the Philippines Sea convection to the South China Sea. In this way, the convection and pressure changes during the heavy rainfall event show the consistent structures of the surface wind variation. At 0000 UTC 17 Jul, a southwesterly flow toward the Philippines Sea is apparent between the western Borneo high and northwest Pacific low, which is an indicative of wind forcing flows from high-pressure regions to low-pressure regions.

Besides, the MWSL geopotential fields on 17 Jul featured an upper-level ridge over South China Sea and an upper-level trough over Philippines Sea. We find that the heavy rainfall event on Jul 17 over Kota Kinabalu is intensified simultaneously. It is considered that the upper-level low pressure in the South China Sea is related to the rainfall. The center of a mobile cyclone was located on the northwest of Philippine Sea, which was believed to be the aftermath effects from Typhoon Haitang. The storm formed as a poorly organized depression at about 280 km west of Marcus Island, Japan at 1200 UTC 11 Jul. By 1800 UTC 13 Jul, it reached a high, destructive tropical storm strength and continued to gain in strength as it moved westward to Philippines Sea on 15 Jul. At 0000 UTC 17 Jul (Fig. 3), the southwesterly flow towards the eastern coast of Borneo was intensified. The cyclone with a center geopotential height of less 5000 gpm was maintained at the Philippines Sea until 19 Jul 2005. At 0000 UTC 19 Jul (Fig. 3), another cyclone with center geopotential height of less than 14,000 gpm was observed at the Philippines Sea near 130°E. It maintained at the same location with an intensified central gpm of less than 8000 gpm at 0000 UTC 20 Jul 2005.

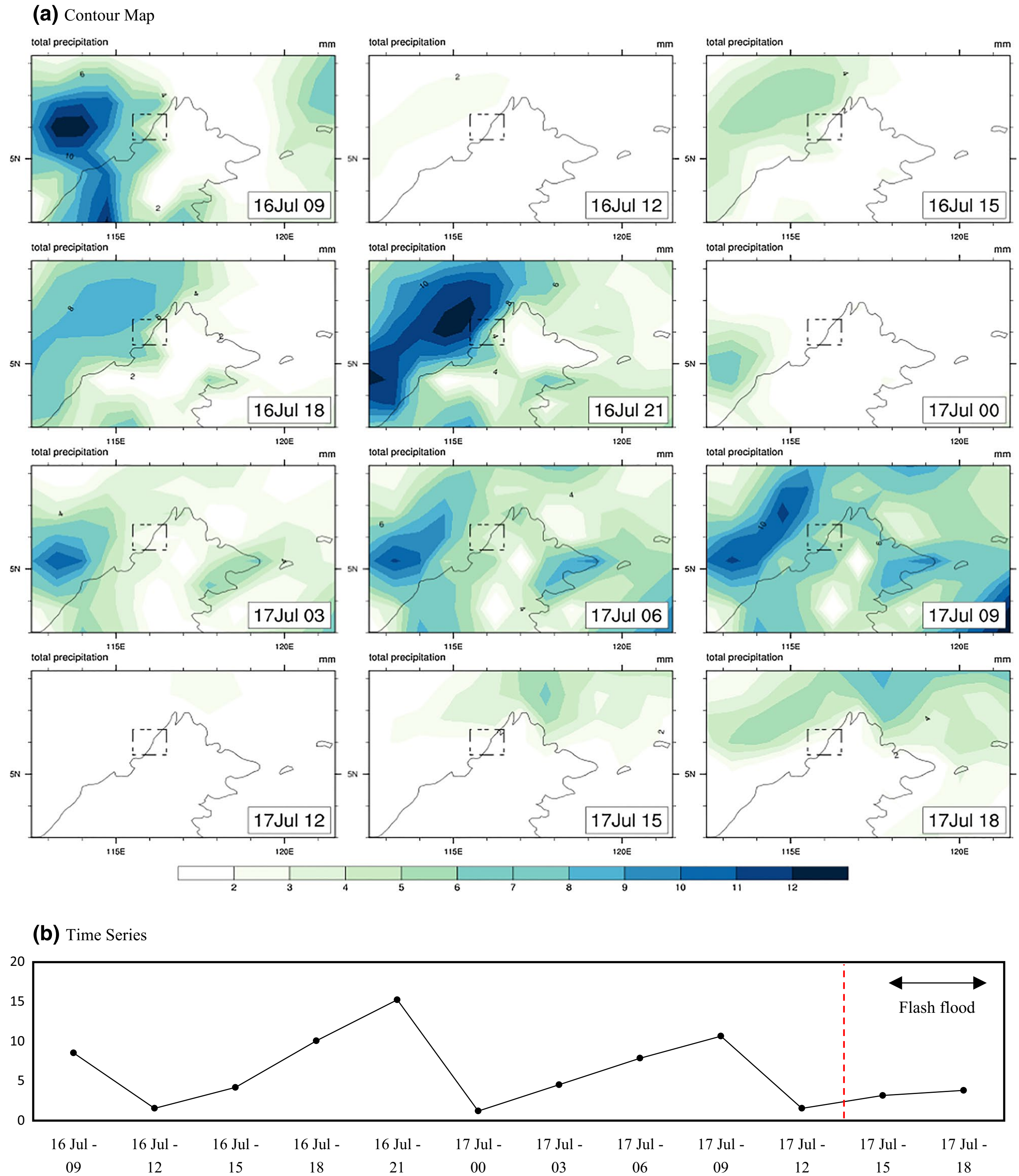

Fig. 2 Observed total precipitation (mm) in **a** contour map and **b** time series obtained from ERA-Interim Reanalysis at interval 3-h accumulated total precipitation from 0900 UTC 16 Jul until 1800 UTC 17 Jul. The dashed line box on **a** represents the KK area. The total precipitation shown on **b** is extracted at the grid point nearest to KK. The red dotted line on **b** represents the time reported for heavy rain and followed by flash flood occurrence in KK from local news

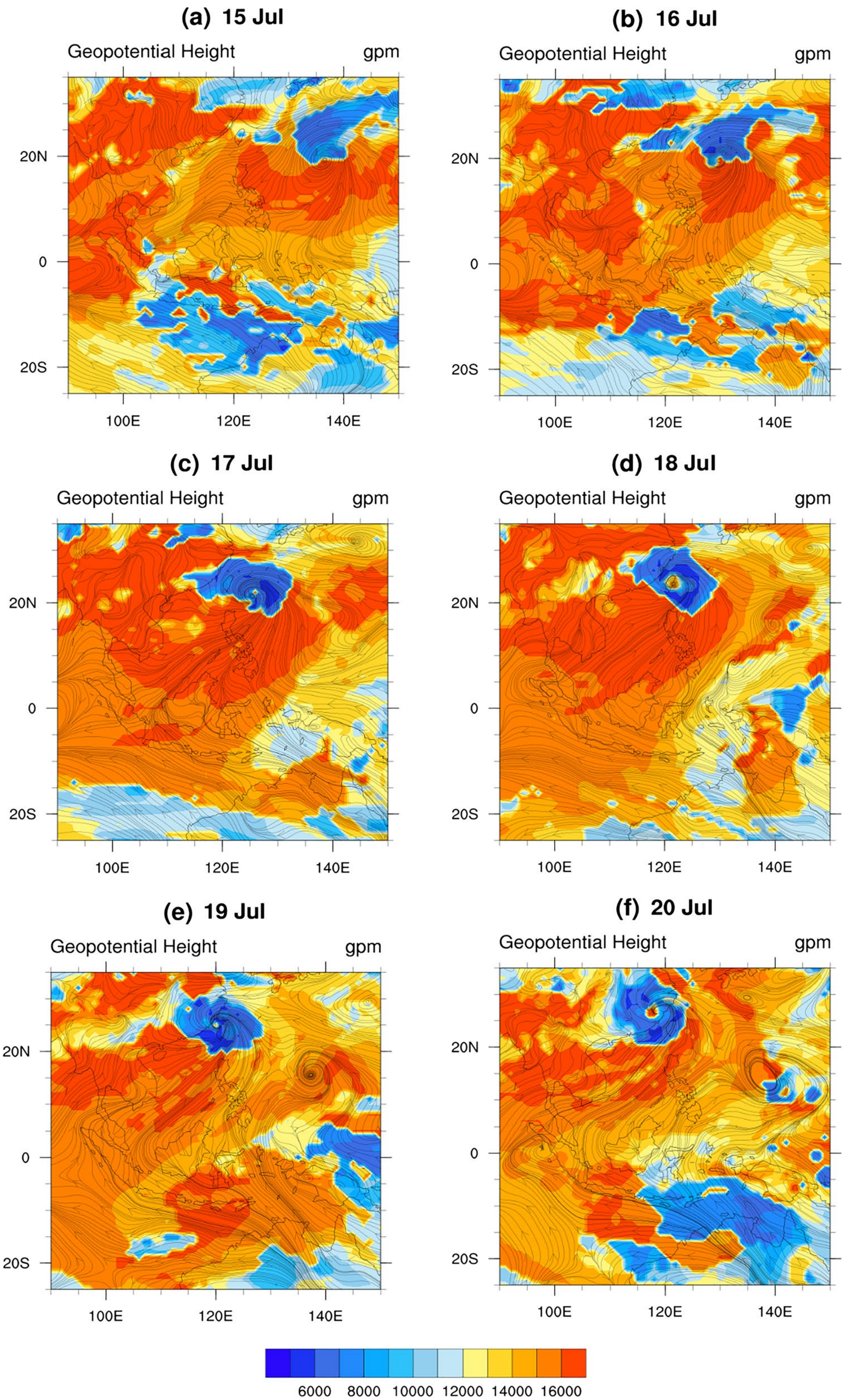

Fig. 3 Streamline plot of FNL analysis of surface wind vectors at 1000 hPa and geopotential height at MWSL (unit: gpm) from 15 to 20 Jul 2005 valid at 0000 UTC. The geopotential height field before (15 Jul) and after (20 Jul) the heavy rainfall event (17 Jul) are shown for comparison

Figure 4 shows the geopotential height and wind vectors at different pressure levels of 300, 500, and 850 hPa analyses from the NCEP FNL data at 0000 UTC 17 Jul 2006 with the precipitation intensity at its maximum at Kota Kinabalu. No significant trough or ridge was observable at high level of 300 and 500 hPa. The patterns of iso-geopotential lines

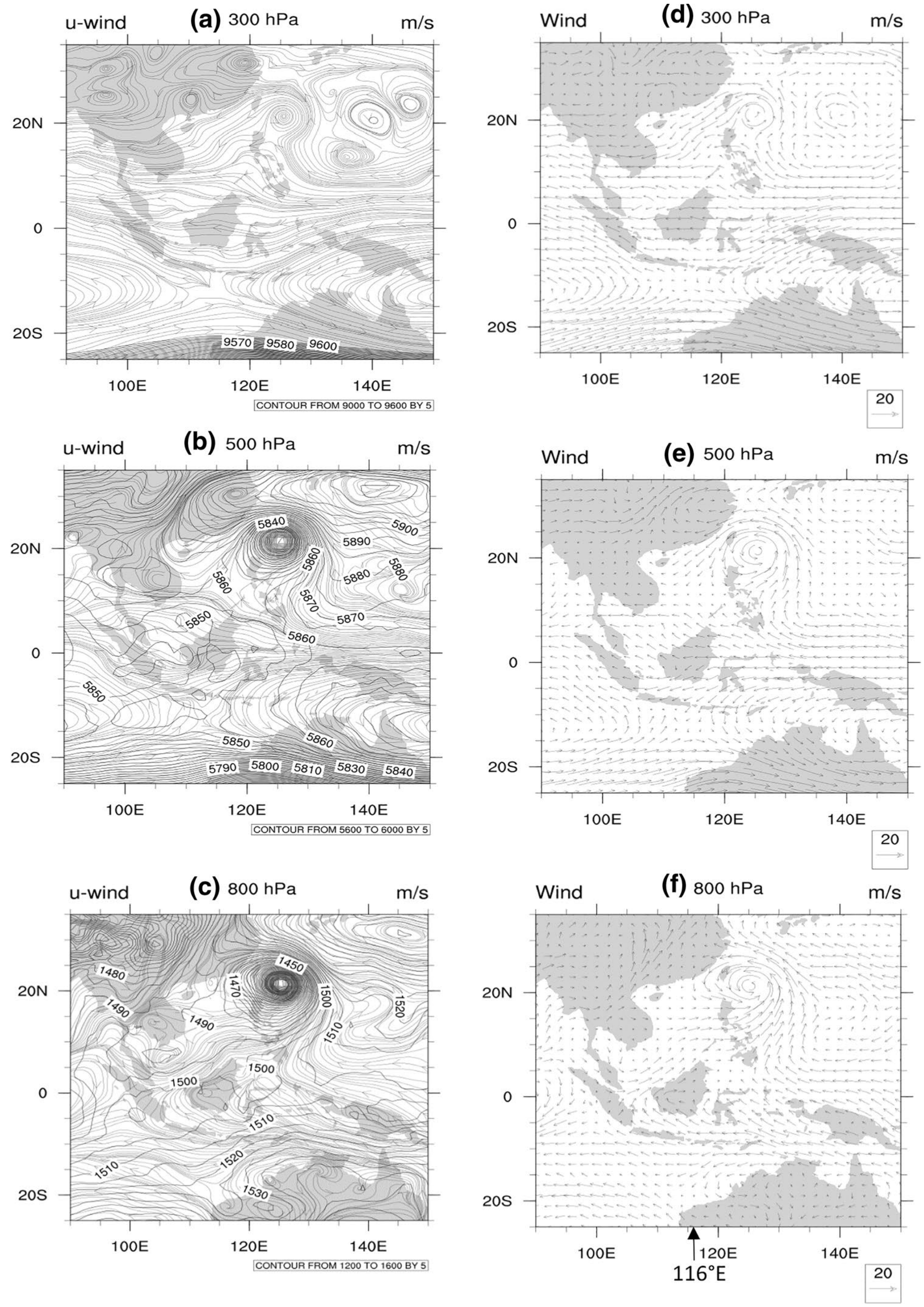

Fig. 4 The FNL 300 hPa (top), 500 hPa (middle), and 850 hPa (bottom) geopotential heights (gpm) and wind vector and its magnitude (ms^{-1}; solid lines), valid at 0000 UTC 17 Jul 2005. **a**–**c** The streamline plot of zonal and meridional winds overlaid on the geopotential height in gpm. **d**–**f** The wind vector plot of u-component and v-component winds. The marker represents vertical cross section along 116°E (KK city) to put Fig. 5 in context

at 300 hPa are similar to those at 500 hPa, except that geopotential fields at upper-level are more stably consistent. At 850 hPa, a low-pressure center was formed and observed near 120°E of Philippines Sea. It is also considered as trough which is indicated by lower geopotential height fields. A short-wave of trough is observed over the Sabah region and a short-wave of ridge was observed to the east-northeast of Philippines Sea (Fig. 4 see bottom-850 hPa). This low-pressure system formed in the lower troposphere, leads to wind blowing in southwest direction from Borneo to Philippines. The increase in height causes the low-pressure tongue to expand onto eastern regions of Philippines Sea and formed several centers of cyclone at 300 hPa. Thus, at the level close to surface, an anticyclone was evident in the northeast of Philippine Sea with higher pressures over Sabah and Philippines regions. This is consistent to the contrary of upper-level trough at MWSL observed over Philippines Sea and upper-level ridge observed over South China Sea. Over the South China Sea, it is also known as the upper-level ridge lower level cyclone. Upper-level lows are closed cyclonically circulating eddies in the middle and upper troposphere. They are sometimes also called cold drops, because the air within an upper-level low is colder than in its surroundings. Therefore, colder air drops and warmer air rises to form a convective system resulting in clear skies and rising pressure at the surface. When the pressure continues to rise for clearing skies until a point at its highest pressure, cloud thickening is the most intense and eventually leads to outbreak of heavy precipitation with falling pressure.

Over the Philippine Sea, the upper-level trough can be explained by the classical process of the life cycle of an upper-level low. It can be separated into four stages: upper-level trough, tear-off, cutoff, and final stage. In the first stage, the field of the absolute topography is characterized by an increase of the amplitude of the potential wave and sometimes also by a decrease of the wavelength. The same development takes place for the temperature wave. In the northern hemisphere a southward deviation of the isohypses and isotherms of the upper-level trough can be observed leading to a deepening of the trough. In the second stage, the trough starts to detach from the meridional stream. As a consequence of the further increase in the amplitude of the waves (further deepening of the trough) the cold air from the north streaming to southern regions will be cut from the general polar flow and the warm air from the south streaming to northern regions will be cut from the general subtropical flow. The consequence of this process is the development of a cold upper-level low within the southern part of the trough. The circulation of the low is characterized by closed isohypses and an eddy in the wind field at 500 hPa (Fig. 4, see panel 500 hPa). In contrast to the previous stage, the tie-off is finished and the upper-level low is now much more pronounced. The wind field at 500 hPa shows a well-developed closed circulation in the area of the former trough which in the ideal case is cutoff from the general meridional flow. In the final stage, the air near the surface is warm and the circulation is slowed down by the friction. The convection brings warm air and the effect of the friction upwards. Within the upper-level low there is convection, unless the surface is very cold. This could happen for Northern or Southern Antarctica regions but the convection system is highly likely to happen over the tropical region near equator. Considering the large area of upper-level low, the baroclinicity is strong and the surface is warm. Further, a low deepens on the surface and the cyclone moves counterclockwise around the large upper-level low. This development lasted for at least 3 days from 17 Jul until 19 Jul 2005.

When the amplitude of a wave pattern aloft is large, troughs and ridges are deep (Fig. 4 see panel 300 hPa). During these conditions, cold polar air moves southward filling into the trough and warmer tropical air moves north into the ridge. This condition is referred to as meridional flow. Eventually, the amplitude increases until the wave breaks up, leaving pools of cooler air at the lower level and warmer air at the upper level. Meridional flow tends to result in stormy weather at the surface for the pronounced wind fields near 15°N at 300 hPa. Besides, a jet stream was also observed at the eastern coast of Sabah region. The advection of moist and warm air due to the low-level southwesterly flow into the Sabah region which is a favorable environment for heavy rainfall events over the Sabah coastal areas.

Figure 5 shows the vertical cross section along the 116°E for 6-h accumulated valid until 0600 UTC 17 Jul 2005. A significant convergence was observed near Kota Kinabalu (5.98°N) at the surface around 1000 hPa. At the upper level around 50 hPa, a significant divergence area is formed where an updraft is speculated to start detrain. At this level, the divergence is formed near 6°N with a forcing nearly 3×10^5/s. The convergence is the strongest near the surface where it covers from 5°N to 7°N centered at 6°N. The convergence shifts towards north with heights and forms another center at 500-hPa. Further up, another strong convergence center is formed at 70 h-Pa but at this level the convergence area is substantially greater in size which spans from 3°N to 5°N and 7°N to 9°N. No significant cold-pool of induced meso-high was found near the surface at Kota Kinabalu area. Instead, cold air mass was concentrated at the upper level from 70 to 150-hPa with potential temperature less than 200 K. This area of cold air mass is accompanied by strong wind fields both in zonal and meridional wind for which reaches to a maximum of 32 m/s and 8 m/s, respectively. The southerly wind flows into the Borneo area and turns into an updraft near the Kota Kinabalu area, where the surface convergence forms. The convective instability is identified below 400 hPa, south of Kota Kinabalu.

5 Mesoscale numerical model description and experiment design

The numerical experiment was executed using the WRF version 3.9, which was developed at the National Center for Atmospheric Research (NCAR) operated by the University Corporation for Atmospheric Research (UCAR). It is a fully compressible non-hydrostatic model with an Arakawa C-grid staggering system. The model domain covers most of the Sabah region. According to the geographical regionalization of Sabah, four representative climate regions in the model area are selected for the analysis of the simulated results, i.e., (a) Kota Kinabalu (KK) (b) Sandakan (SDK) (c) Keningau (KEN), and (d) Tawau (TWU). Figure 6 shows the model domain with topography and four climatic subregions. The centre of the model domain is at 5°N, 118°E with 82 north–south points and 106 east–west points and a horizontal grid spacing of 45 km is used. The model configuration

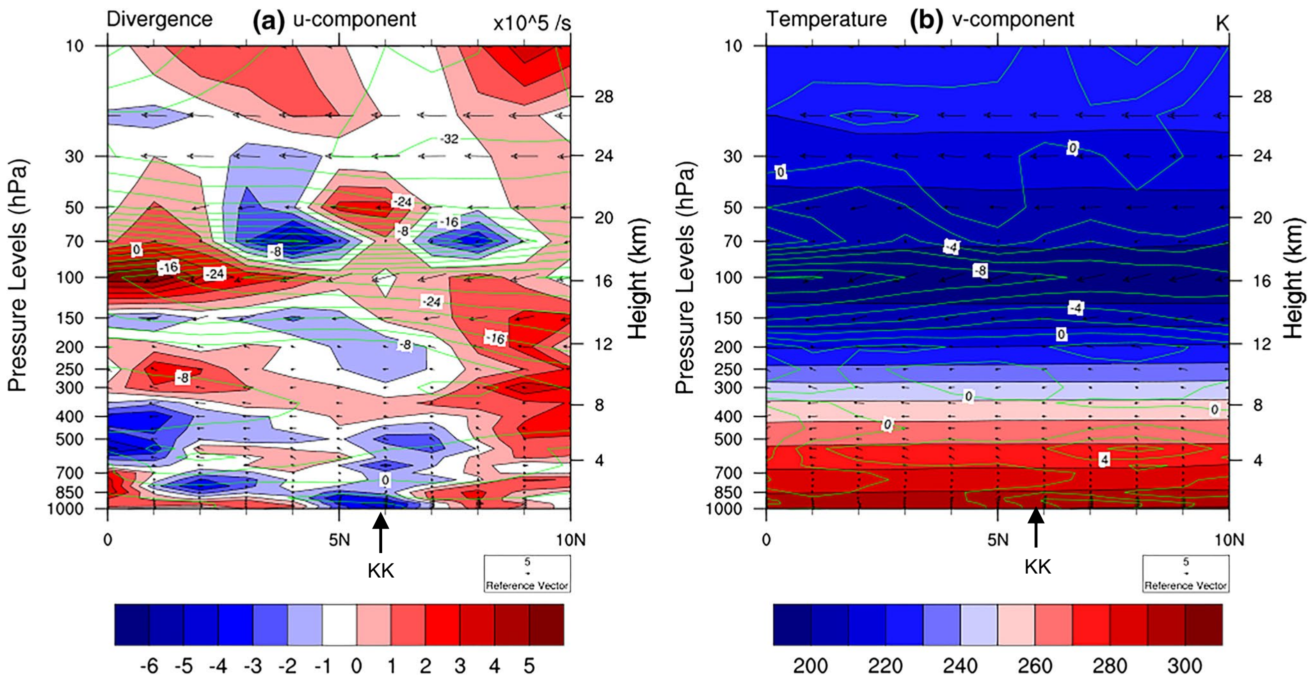

Fig. 5 Vertical cross sections along 116°E at 0000 UTC 17 Jul 2005 obtained from FNL, for **a** zonal wind speed (m/s, line contour) and divergence (10^5/s, shaded) and **b** meridional wind speed (m/s, line contour) and air temperature (K, shaded)—right panel. The vector on both panels represents wind speed. The positive/negative value for u-component represents east/west direction and for v-component represents north/south direction. The marker represents KK city

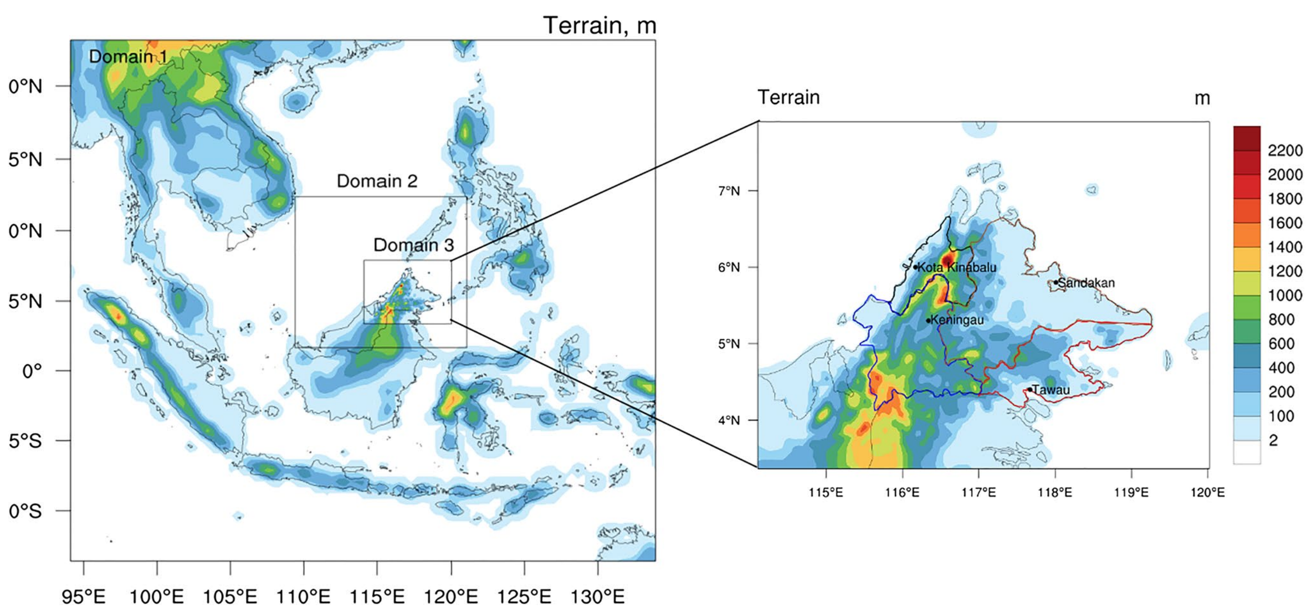

Fig. 6 Mercator conformal map projection of the Sabah region with the terrain heights at a 45-km resolution for Domain 1, 15-km (Domain 2), and 5-km (Domain 3). On Domain 3, the black dot (solid line color) represents the administrative capital location (area coverage) for each subregion in Kota Kinabalu (black), Sandakan (sienna), Keningau (blue), and Tawau (red)

consists of one-way interactive triple-nested domains with a Mercator conformal map projection (Table 3).

All domains have 27 vertical layers with a terrain following sigma coordinate, and the model top is 50 hPa. In Domain 3, the detailed features of the complex orography over Sabah are resolved. For example, terrain heights greater than 1.4-km appeared along the Kinabalu mountain and the central part of the eastern Kota Kinabalu (see Fig. 6).

Table 3 Domain configuration of the three nested domain centered over Kota Kinabalu, Malaysia

Domain	Domain 1 (D1)	Domain 2 (D2)	Domain 3 (D3)
Time step (s)	180	180	180
End index in West–East	100	88	133
End index in South–North	94	82	103
Number of vertical eta levels	27	27	27
Top pressure (Pa)	5000	5000	5000
Number of metgrid levels	27	27	27
Number of vertical soil levels	4	4	4
Grid length in x (km)	45	15	5
Grid length in y (km)	45	15	5
Geographical data resolution (min)	10	5	2
Region cover	Southeast Asia	Borneo	Sabah

Note that Domain 1 is too small for describing the synoptic features associated with the heavy rainfall. The purpose of this study is to examine the capability of the WRF model to reproduce the flash flood heavy rainfall, we employed a smaller domain than that covering the synoptic-scale flows. The synoptic scale conditions were therefore provided by the FNL data. Besides, the time step run is also reduced to 180 s unlike the rule of thumb of 6/1000 of dx or dy. This is because to avoid the segmentation errors of CFL, which are generally caused by vertical winds that are too fast for WRF to solve. Particularly, they generally happen over high mountain peaks (Molg et al. 2009), which is unlikely to avoid in the case of the study area. Even though vertical winds are slow compared to horizontal winds, grids cells have coarse resolution for vertical layer compared to their horizontal dimensions. Therefore, reduced time steps within the enhanced resolution of ARW is adopted in the current study to reduce the impact of vertical velocity damping which could unnecessarily suppress strong updrafts or downdrafts associated with significant gravity wave propagation and breaking (Hahn 2007).

Note that cumulus parameterization was not used in the 5-km grid model where convective rainfall generation is assumed to be explicitly resolved. Details of the physics scheme used are depicted in Table 4. We selected this combination of physical schemes based on previous studies to optimize the WRF performance on the simulation of flash-flooding heavy rainfall event (Hong and Lee 2009). Besides, this model configuration was also adopted in other studies such as in tropical region of Singapore (Singh et al. 2015) for monsoon and inter-monsoonal seasonality, in South China Sea (Haghroosta et al. 2014) for typhoon simulation, and in Peninsular Malaysia (Ardie et al. 2012) for heavy rainfall episodes. Initial and boundary conditions were derived from the NCEP FNL, without specific assimilation of observational data. The lateral boundary condition was updated at 6-h interval.

In this paper, the flash-flooding heavy rainfall event during 16–18 Jul 2005 is mainly simulated and analyzed. A total of three experiments were conducted to fully cover the period of the flash-flooding event with at least 1 day (24-h) for initial spin-up. The simulations are designed so that the common simulation period is covered in all experiments for the day before the event (16 Jul) and the day after the event (18 Jul). Each experiment was initiated at different starting time but ended at the same ending time, i.e., E1 starts at 0000 UTC 15 Jul 2005 and ends at 0000 UTC 19 Jul 2005 for a total of 4-days accumulated run period. The time for

Table 4 Physics configuration of the three nested domain for WRF-ARW model v3.9

Domain	D1	D2	D3	Note	References
Microphysics	6	6	6	*WSM 6-class graupel scheme* A new scheme with ice, snow and graupel processes suitable for high-resolution simulations	Hong et al. (2004) Hong and Lim (2006)
Cumulus parameterization	1	1	0	*Kain-Fritsch (new Eta) scheme* Deep and shallow sub-grid scheme using a mass flux approach with downdrafts and CAPE removal time scale	Kain (2004)
Planet boundary level	1	1	1	*YSU scheme*	Hong et al. (2006)
Shortwave radiation	1	1	1	*Dudhia scheme* Simple downward integration allowing for efficient cloud and clear-sky absorption and scattering	Dudhia (1989)
Longwave radiation	1	1	1	*RRTM scheme* Rapid Radiative Transfer Model. An accurate scheme using look-up tables for efficiency. Accounts for multiple bands, trace gases, and microphysics species	Mlawer et al. (1997)

starting and ending for each experiment is shown in Table 5. The evolution of the weather system from 16 to 18 Jul representing the day before (B), during (D), and after (A) the flash flood, is mainly analyzed in this paper.

6 Modelled results

For the validation of modelled results from WRF, we selected three gridded precipitation products namely TRMM, PERSIANN-CDR, and CHIRPS. Figure 7 shows the comparison of WRF-modelled daily precipitation with the three selected gridded products for the five study areas. All precipitation values shown in Fig. 7 are area-averaged, as different study areas have different area coverage. In general, all gridded products revealed the peak of the extreme precipitation amount occurred on 17 Jul particularly in KK. The gridded products also confirmed the occurrence of the heavy rainfall event during this period where almost all products observed higher than normal precipitation level (see dotted line on Fig. 7) especially in KK and Keningau region.

Among all regions, our modelled results in KK region simulated the highest precipitation amount particularly on 16 and 17 Jul, which is corresponding well to the observation from TRMM and PERSIANN-CDR. Particularly, E1 has best captured the initiation, intensification, and deceleration of the rainfall activity. The second highest precipitation amount was simulated in Keningau region but the simulation of all experiments failed to capture the evolution of the rainfall activity. When all gridded products show that the peak was observed on 17 Jul, our modelled results in Keningau have captured the peak on 16 Jul which is on a 1-day lag behind the observation. We believe the discrepancy is possibly due to the timing shifts withdrawn when looking at the 1-day precipitation amounts. The timing shifts become significant often when the modelled result reproduced the

Table 5 Experiment name, starting and ending time to test the sensitivity of modelled results to different run period

	Starting Time	Ending Time	Run Period	13 Jul	14 Jul	15 Jul	16 Jul	17 Jul	18 Jul
E1	0000 UTC 15 Jul 2005	0000 UTC 19 Jul 2005	4 days				B	D	A
E2	0000 UTC 14 Jul 2005	0000 UTC 19 Jul 2005	5 days				B	D	A
E3	0000 UTC 13 Jul 2005	0000 UTC 19 Jul 2005	6 days				B	D	A

[Symbol B: before, D: during, A: after the flash flood]

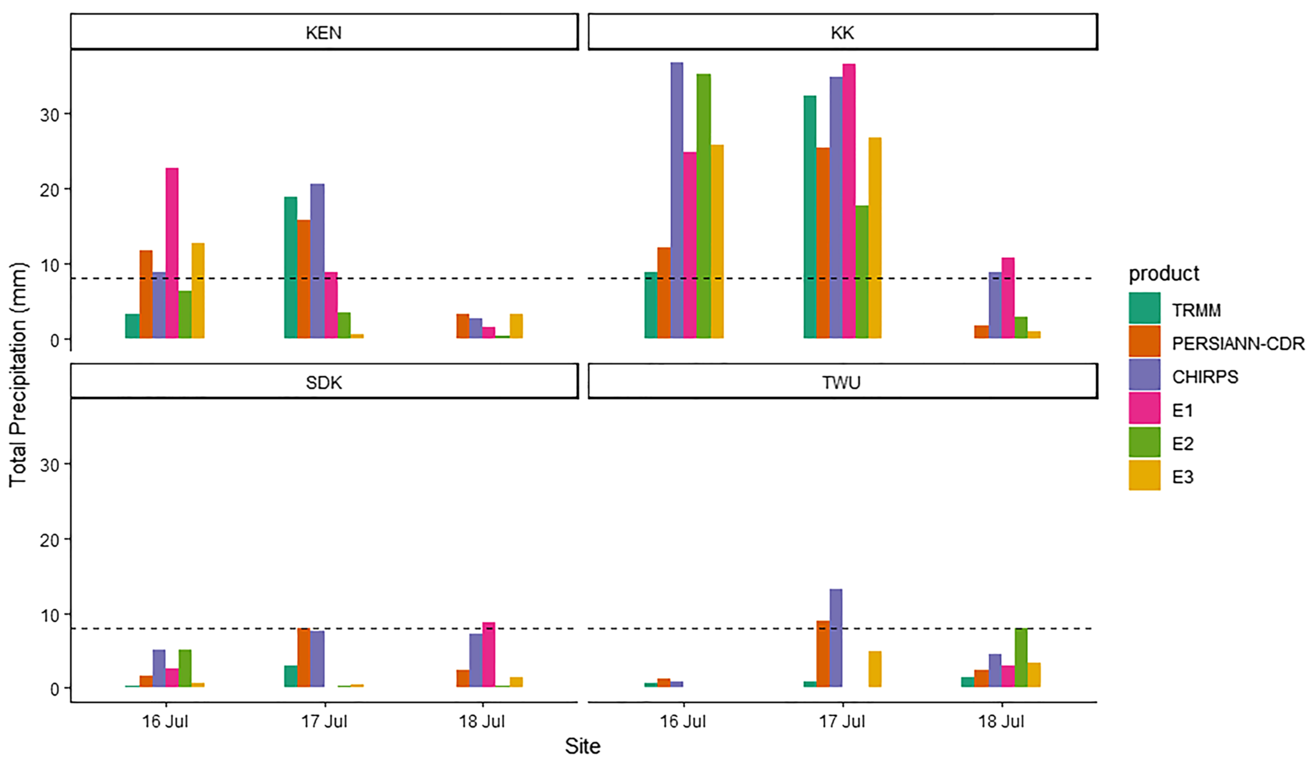

Fig. 7 Bar chart of total precipitation in mm obtained from TRMM, PERSIANN-CDR, CHIRPS, and WRF (E1, E2, E3) for the four study areas from 16 to 18 Jul 2005. The dotted line represents the normal daily precipitation level (~8 mm) in Sabah

heavy rainfall event with a time lag of several hours. For example, the 3-h peak in Keningau was simulated at 1500 UTC 16 Jul (E1), 0900 UTC (E2), 1200 UTC (E3) which lags by 18 ~ 24 h to that of TRMM at 0900 UTC 17 Jul. This time delay issue is also reported by other model results of heavy precipitation event (Jee and Kim 2017; Maussion et al. 2011). However, this issue is not significant in KK region because all experiments have simulated the peak at 0900 UTC 17 Jul (E1, E2) and 1500 UTC (E3), which leads by only 6 h to that of TRMM at 1500 UTC 17 Jul. Another possible discrepancy is due to the considered spatial subset that is different with respect to observed precipitation patterns. Although the lat/lon from the modelled result has been fixed to match the corresponding lat/lon from the gridded products when extracting the precipitation amount, the spatial mismatch between the simulated precipitation area to that of gridded products remains uncertain especially when downscaling is done in regional climate model. As a whole, the WRF results generally simulated the heavy precipitation event in KK but we somehow believe that the simulation lags by some delays especially in other regions. It is worth to mention that the WRF E1 result reached the highest precipitation amount of 37.0 mm in KK on 17 Jul; 25.0 mm in KEN on 16 Jul, while other areas (SDK and TWU) do not receive remarkably high rainfall amount both from the gridded products and WRF modelled results.

Figure 8 shows the boxplot of total precipitation between the gridded products and simulation results separated by (a) region (b) region and date. On the whole, the distribution of the total precipitation between the gridded and simulated is similar where both data sets have the highest dispersion in KK and relatively lower dispersion in SDK and TWU.

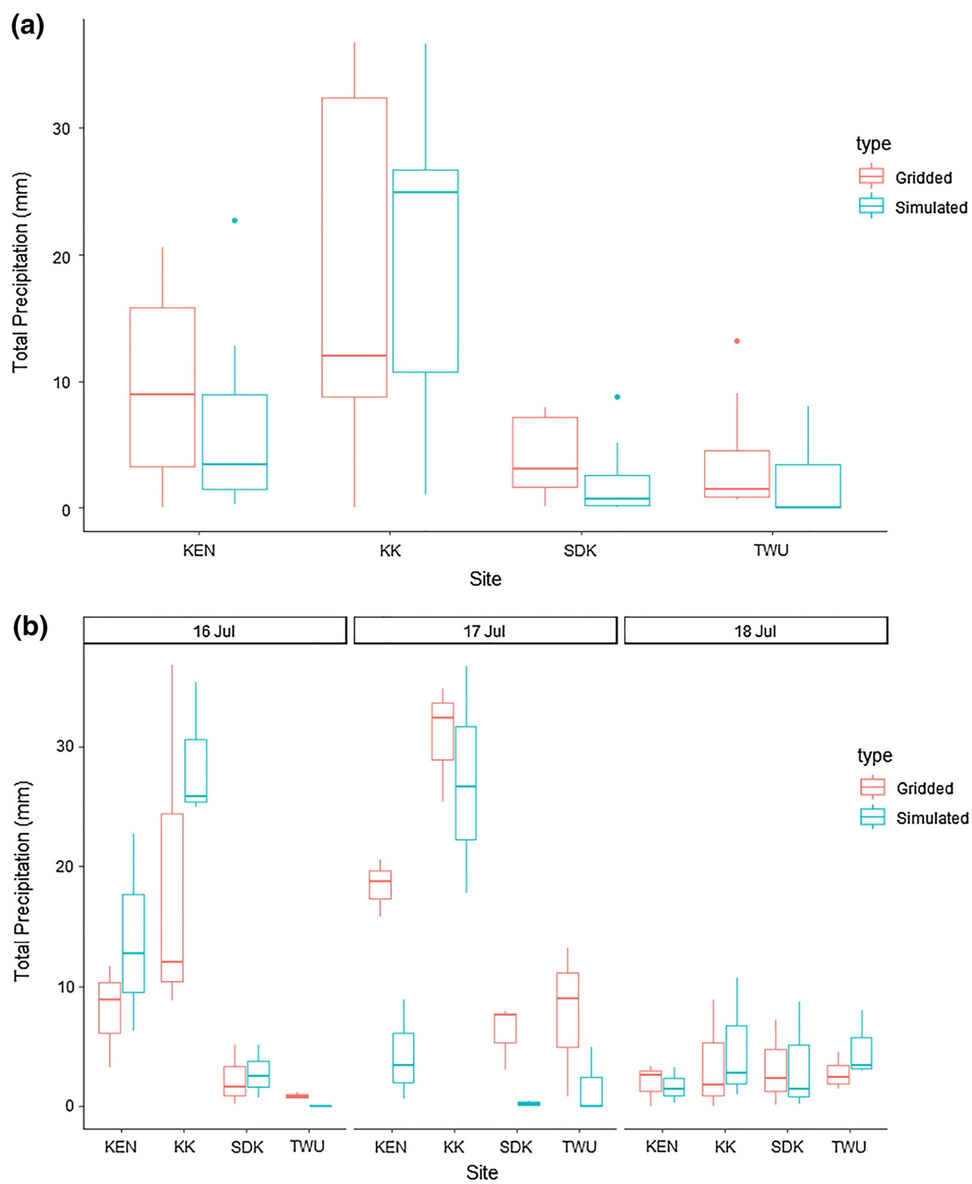

Fig. 8 Boxplot of total precipitation (mm) averaged from gridded products (TRMM, PERSIANN-CDR, and CHIRPS) and simulated products (E1, E2, and E3). **a** The total precipitation for the four study areas and **b** separates with respective to the date

Considering the large difference between the gridded products, we further compared our modelled results with the total precipitation averaged from the three gridded products. Similarly, the total precipitation from WRF simulation E1, E2 and E3 is also averaged for easy comparison. On average, the mean value from the simulation basically agrees well with the gridded products with slight underestimation/overestimation in all regions. The overestimation/underestimation is about 2.8 mm at most, which we believe the totality of the WRF simulation have successfully reproduced the resemblance with the observation. The standard deviation is the highest > 14 mm in KK region, followed by KEN (> 8 mm) and relatively low < 5 mm in SDK and TWU region. We believe this was attributed to the complex topography features associated with the region itself. KK and KEN region are both located near the high, complex terrain areas (e.g., Mount Kinabalu and Crocker Range) while the two topography features of the other two regions are rather flat. This is also supported by the gridded products where the standard deviation in KK and KEN is also relatively higher than SDK and TWU. To look into detail on the evolution of the total precipitation, we refer to Fig. 8b. On the first day (16 Jul), nearly all simulated results in different regions overestimated the total precipitation with the highest maxima > 30 mm was simulated in KK region. On the second day (17 Jul), all simulated results underestimated the gridded products. On the third day (18 Jul) where the heavy rainfall activity has receded, good agreement between the gridded products and simulated results is observed for all regions. Details of the statistical measures on each day are given in Table 6.

For the spatial distribution, we selected TRMM-gridded product to compare our WRF modelled results due to its high temporal resolution. Figure 9 shows the 5-km grid experiment from E1, E2, and E3 and TRMM rainfall product, capturing the evolution of the daily rainfall from 16 to 18 Jul. In Fig. 9j–l, an observed rainstorm from the gridded data on 16 Jul is evident over the KK region of Sabah (see the shapefile highlighted). In addition, the rainstorm persisted until 17 Jul with the rainfall pattern slightly shifted from west to east. The simulated case on Fig. 9a–c shows the similar features, with large area of rainfall activity observed over the KK and Keningau region on 16 Jul and 17 Jul. The simulated case E1 also shows the heavy rainfall shifted to the northeastern coast of Sabah on 17 Jul (see Fig. 9a, b). On 18 Jul, the accumulated rainfall in Sabah obtained from both WRF and TRMM was low with very little precipitation amount. From the simulation result, it is clear that this major event has caused significant amount of rainfall over the KK region in Sabah. Considering the complexity of atmospheric modeling and the challenges in obtaining reliable and accurate in situ data with which to evaluate such models, these simulations seem quite reasonable. The modelled results captured the similar rainfall distribution as observed by the gridded product where large area of rainfall activity was in agreement to each other at nearly the same place and time. Besides, our findings show that the WRF simulation overestimated the total precipitation obtained from gridded products (see Figs. 7, 9). For example, the simulated rainfall E1 in KK on 16 and 17 Jul reached almost 25.0 mm and 40.0 mm respectively, while other gridded products (e.g., TRMM, PERSIANN-CDR) observed relatively low precipitation amount. It is also obvious to notice that many locations receive remarkably high rainfall amount of more than 100 mm in the simulated case on 16 Jul and 17 Jul but none as high as 100 mm was observed in the TRMM observation (see Fig. 9). This is likely due to the complex topography features of the location. The domain that covers the Sabah region has complex orographic and geographic features, such as a mountain range close to the city and a land–ocean boundary (see Fig. 10). Similarly, findings are also reported in other studies that modelling of flash-flood events in tropical areas often suffers from high meteorological and topographic complexity (Rogelis and Wener 2018; Deng et al. 2015).

Considering the totality of the simulation from E1 to E3, the modelled results have confirmed the occurrence of the heavy rainfall event during this period except for some mismatch in terms of spatial and temporal. Given that all three experiments were initialized at different times, they proved that the high precipitation amount in KK region during this major event is not a random occurrence. For example, all experiments have simulated great amount of precipitation in KK on 16–17 Jul, which is associated to the actual flash flood period. When the flood began to recede on 18 Jul, all experiments simulated the deceleration of the major event at nearly the same time. Nevertheless, the small differences in the modelled results between experiments do exist and we

Table 6 Average and standard deviation of total precipitation calculated from the gridded products (TRMM, PERSIANN-CDR, and CHIRPS) and simulated results (E1, E2, and E3) in each region

Total Precipitation (mm)	KK	SDK	KEN	TWU
16–18 Jul				
Gridded	17.9 ± 14.5	3.9 ± 3.1	9.4 ± 7.7	3.8 ± 4.4
Simulated	20.2 ± 14.3	2.2 ± 2.9	6.6 ± 8.4	2.2 ± 4.5
16-Jul				
Gridded	19.2 ± 15.3	2.3 ± 2.5	8.0 ± 4.3	0.9 ± 0.3
Simulated	28.7 ± 5.8	2.8 ± 2.2	13.9 ± 8.3	0.0 ± 0.0
17-Jul				
Gridded	30.9 ± 4.9	27.5 ± 2.7	6.2 ± 2.4	18.4 ± 6.3
Simulated	27.0 ± 9.4	0.3 ± 0.2	4.3 ± 4.2	1.7 ± 2.9
18-Jul				
Gridded	3.6 ± 4.7	3.2 ± 3.6	2.0 ± 1.8	2.8 ± 1.6
Simulated	4.8 ± 5.2	3.5 ± 4.6	1.7 ± 1.5	4.8 ± 2.8

believe they are related to the different initial and boundary condition within the domain. Within the data simulated in this paper, the modelled results initiated from near-present of a major event seems to outperform those initiated from far-present. However, more work in regional climate modelling in future is expected to answer and support this hypothesis.

To scrutinize the WRF simulation analysis and given that E1 has best captured the evolution of the rainfall activity, we further identified several locations in Sabah that receive heavy precipitation amount using the modelled result obtain from E1–D3. Hence, the following results and discussion hereinafter refer to and focus on E1–D3 only. To identify these locations, first we extracted the total precipitation amount from E1 at each pair of lat/lon coordinates. Then, we define heavy rainfall location as coordinates within Sabah region that receives high total accumulated precipitation amount of at least 150-mm from 16–18 Jul. These locations are summarized in Table 7 and visualized on Fig. 10. Overall, a total of 6 locations are identified where 3 are from KK region and 3 from Keningau region.

Over the KK region, the three locations are identified at Mount Kinabalu (A1), Tuaran (A2), and Tambunan (A3). They are all near the complex topography of Mount Kinabalu (> 2200 m a.s.l.) (see Fig. 10). The maximum total rainfall was simulated in A1 with a remarkably high total precipitation of 201.31 mm. It is also associated with a total of 8 peaks of hourly rainfall with the maximum at 0600 UTC 18 Jul (32.75 mm/h). Besides, A2 and A3 also simulated considerable total precipitation amount of 149.15 mm and 128.66 mm, each with 3 and 5 peaks, respectively. All these three locations are located near the vicinity of KK city where the landslides and severe flash flood had occurred on 17 Jul 2005. Though the respective max hourly rainfall of each location does not occur at the same time, the overall consequences can be severe to the city considering the time shift effect in the modelled result. Thus, from Table 7, the WRF results suggested that the severe flash flood event in KK city was partly rooted to several major heavy rainfall events occurring at different times within the KK region. The affected areas include of Mount Kinabalu (A1), Tuaran (A2), and Tambunan (A3). Meanwhile, over the Keningau region, another three heavy rainfall locations are identified at Tenom (A4), Sipitang (A5), and Sapulut (A6). These locations might not be located exactly near Mount Kinabalu like those in KK region, but their topography feature is yet complicated as they all lie along the Crocker Range (2076 m a.s.l.) The maximum total precipitation 173.92 mm was simulated in A6 with the max hourly rainfall occurring at 1200 UTC 16 Jul for 84.69 mm/h.

Figure 11 shows the time series of total precipitation and hourly precipitation for the six locations summarized in Table 7. Over the KK region, A1 is the location that receives the highest rainfall amount according to the WRF simulation results. The highest accumulated total rainfall at A1 reached to 201-mm at 0800 UTC 18 Jul. As indicated in the hourly precipitation plot, the location might not have the highest rainfall tendency but the duration of rainfall is long and more frequent as compared to other locations. For example, the first rainfall in A1 started at 0200 UTC 16 Jul and persisted for a period of 4-h until 0500 UTC. An hour later, the second rainfall started at 0600 until 0900 UTC for 3-h. Similar long period of rainfall duration was simulated on 17 Jul in A1 where the first rainfall started at 0100 UTC and persisted until 0500 UTC and the second peak started at 0600 UTC and persisted until 1200 UTC for a total period of 8-h rainfall. Till here, we argue that the long hours of rainfall during these hours is believed to be the possible factor responsible for the flash event hit Kota Kinabalu on 17 Jul 2005. If we compare the incident time reported by most of the local news, the heavy rainfall started since afternoon 17 Jul at around 1400 UTC which nearly coincides with the peak rainfall simulated in A1 except for a slight delay of few hours (see Fig. 11). Similar trend with less numbers of hourly rainfall peak is also simulated in A2 and A3. It is obvious that both locations have three major rainfall occurred separately at different times (see Fig. 11). The previous rain event on 16 Jul was expected to affect the soil saturation and water runoff in the vicinity of KK city. The actual rain event on 17 Jul further deteriorated the situation and eventually caused the flash flood hit the city.

Over the Keningau region, location A4 and A5 have simulated the similar rainfall evolution pattern where the first major rainfall occurred at the morning hours of 16 Jul and the second at the noon hours of 17 Jul. Meanwhile, rainfall in A6 occurred only at the noon hours of 16 Jul. It is worth to highlight that both A4 and A5 are locations in the Keningau region (lower land) that received considerably high precipitation amount for two consecutive days from 16 to 17 Jul, which is the same as A1 (higher land). However, the flooding event in Keningau region was relatively less impactful when compared to Kota Kinabalu region. This is likely due to the catchment area factor as indicated in Table 7. Large catchment area in low land basically collects a lot of water and increasing surface run-off during heavy rainfall. The simulated case A4 and A5 is both located near Padas basin which has the largest catchment area, 9726 km^2 among all other locations. In contrast, A1 is located near Kalimatan basin which has the smallest catchment area, 881 km^2. In addition, the severe flash flood in the vicinity of KK city is further deteriorated due to the prolonged heavy rainfall. The simulated case in A1 clearly depicted the longest rainfall duration of 13-h on 16 Jul and continued with 6–9 h rainfall the next day. In this way, the soil was saturated and the depression storage was fully filled; the continued rainfall immediately produced surface runoff and eventually resulting to flash flood in KK city.

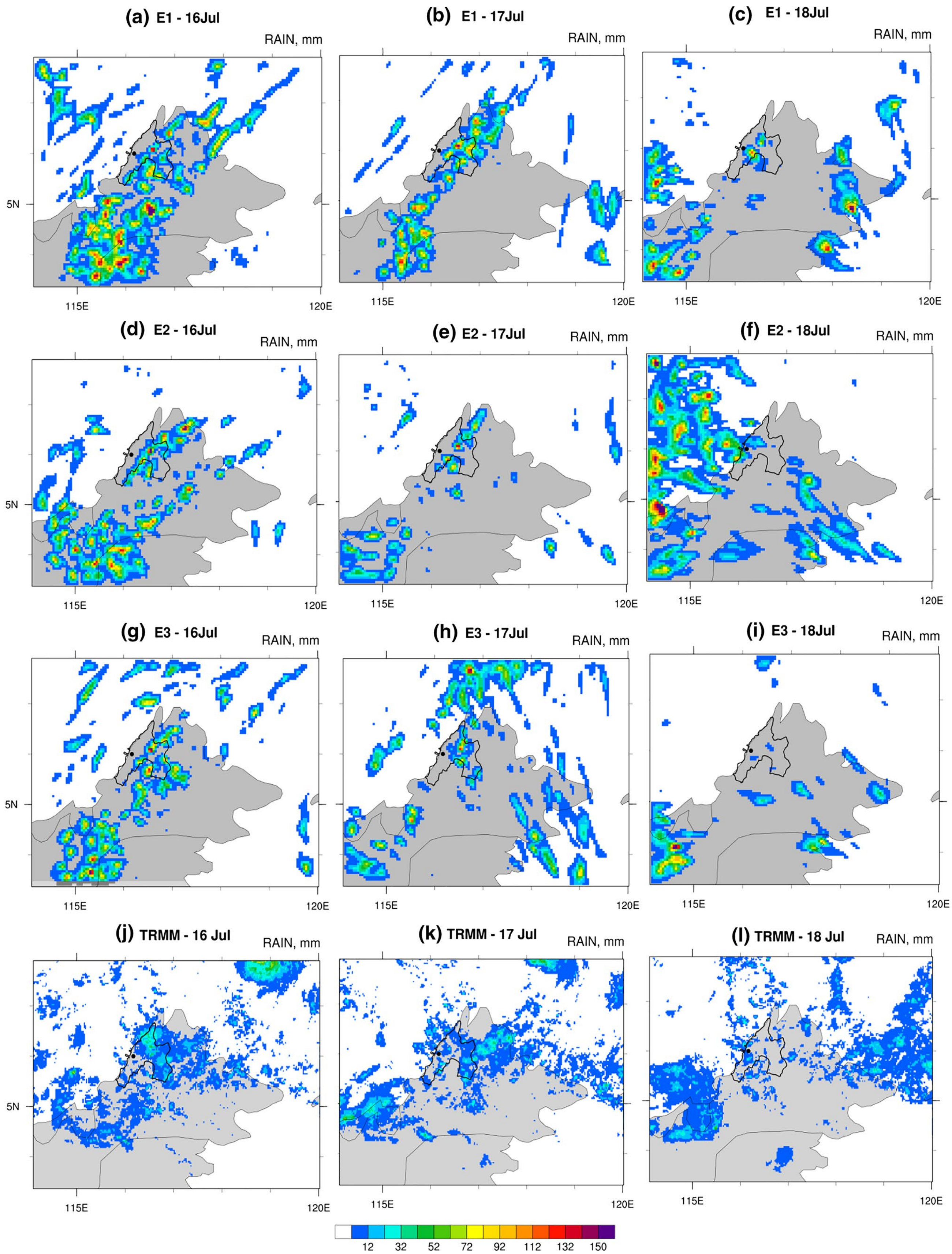
(a) E1 - 16Jul
RAIN, mm
5N
115E
120E
(b) E1 - 17Jul
RAIN, mm
115E
120E
(c) E1 - 18Jul
RAIN, mm
115E
120E
(d) E2 - 16Jul
RAIN, mm
5N
115E
120E
(e) E2 - 17Jul
RAIN, mm
115E
120E
(f) E2 - 18Jul
RAIN, mm
115E
120E
(g) E3 - 16Jul
RAIN, mm
5N
115E
120E
(h) E3 - 17Jul
RAIN, mm
115E
120E
(i) E3 - 18Jul
RAIN, mm
115E
120E
(j) TRMM - 16 Jul
RAIN, mm
5N
115E
120E
(k) TRMM - 17 Jul
RAIN, mm
115E
120E
(l) TRMM - 18 Jul
RAIN, mm
115E
120E
12
32
52
72
92
112
132
150

◂**Fig. 9** Total precipitation in mm on 16 Jul, 17 Jul, and 18 Jul obtained from the WRF simulation and TRMM-gridded product. **a**–**c** Represent E1, **d**–**f** represents E2, **g**–**i** represents E3, **j**–**l** represents TRMM

7 Discussion and conclusion

Three important issues are highlighted in this work: (1) spatial mismatch in triggering location (2) overestimation in precipitation amount between the WRF simulation and gridded products, and (3) possible regional-to-local interaction between tropical cyclone and heavy precipitation event in Sabah.

Although the WRF simulation has captured fairly well the evolution of the heavy rainfall during this major event on regional scale, the spatial mismatch in precipitation pattern at specific lat/lon coordinates remains a big challenge in our work. We acknowledge that the results presented here are to some extent strongly affected by localization error in spatial displacement of the precipitation event on the order of few kilometers. This error is directly related to differences in the fine-scale spatio-temporal features between the simulated and observed convective cell responsible for the event (Fiori et al. 2014). In actual mechanism, the triggering location is contained in a very small region where the total cell width could be less than 5-km. Such fine-scale structure is very challenging for most NWP models operating on the order of 5 km grid spacing. Besides, it is also partly associated to the general deficiency of the mesoscale dynamic processes of the parent model, in reproducing the precise location of prominent local responsible for the persistence of the cell over the city of Kota Kinabalu and surrounding terrain. However, our findings demonstrated a definitive potential in the use of WRF-gridded rainfall for flood simulations in Sabah region, and identified some key issues that require attention to further enhance this potential.

The overestimation in the WRF simulated precipitation amount as compared to the gridded rainfall products observed in this study is likely caused by the complexity of the study area. The complexity is attributed to (1) diverse topography (2) proximity of sea and mountains and (3) local condition of wind circulation. The diverse topography of Mount Kinabalu and Croker Range lies within the Sabah region complicates the spatio-temporal variability of rainfall. Orographic lifting and blocking can tremendously modify rainfall especially in mountainous area over short distances (Lee et al. 2014). Large topographical gradient between sea coast and mountains is typical for Sabah region and the complexity of convective system over coastal and inland areas is very difficult to be sufficiently captured well to describe the local circulation in Sabah region. The local condition of wind circulation especially over the complex topography further hinders the model to accurately quantify windward heavy rainfall. In complex topography, differences in surface radiation generate important thermal contrasts that in turn create local wind regimes. When the model handles these local wind regimes, the simulated precipitation amount tends to be exaggerated (Santos-Alamillos et al. 2013).

In the synoptic scale, the ERA-Interim observation suggested that heavy precipitation over the study area was the most intense on Jul 17, 2005 which coincides with the actual day of the major event. The FNL geopotential analysis indicated a remarkable high pressure at upper level was observed over the central of South China Sea and its westward extension to the Philippines Sea during the heavy rainfall event from 17 to 19 Jul 2005. On Jul 17, the geopotential heights featured an upper-level ridge over the South China Sea and an upper-level trough over the Philippines Sea, for which we believe has intensified the heavy rainfall event. The center of the cyclone was also observed in the northwest of Philippines Sea and associated with wind flowing counterclockwise in the Northern Hemisphere due to the Coriolis Effect. We also studied the variation of geopotential heights at different pressure level and a short-wave trough was observed over the Sabah region at 850 hPa which leads to wind blowing in southwest direction from Borneo to Philippines. It was also noticed that several low-pressure centers were formed at 300 hPa over the Philippine Sea. Over the South China Sea, an upper-level ridge and lower-level cyclone was evident for the pressure rises to its highest pressure, causing cloud thickening and subsequently leads to outbreak of heavy precipitation with falling pressure. The vertical cross section for divergence along 116°E also revealed that a significant convergence was observed near the surface and accompanied by a strong updraft of divergence at upper-level.

In the mesoscale, considering the complexity of atmospheric modeling and the challenges in obtaining reliable and accurate in situ data with which to evaluate such models, the WRF simulations in this work seem quite reasonable. The ability of a triply nested WRF model with a highest resolution of 5-km horizontal grid spacing to predict heavy rainfall in Sabah region from 17 to 19 Jul 2005 was evaluated against three gridded products, e.g., TRMM, PERSIANN-CDR, and CHIRPS. Our modelled result has fairly well demonstrated the initiation, intensification, and deceleration of the major event which agrees well with the observation from the gridded products. The highest total daily precipitation was simulated for about 160 mm near Mount Kinabalu at 1200 UTC 16 Jul 1 day before the major event. This is expected to affect the soil saturation and surface water run-off when heavy rainfall continued to hit the same location the next day and eventually caused flash flood to hit the vicinity of KK city. The simulated result also agrees well with the actual time reported by most local news that the rainfall started in the afternoon 17 Jul at around 1400 and our modelled result shows that several hourly precipitation peaks were simulated

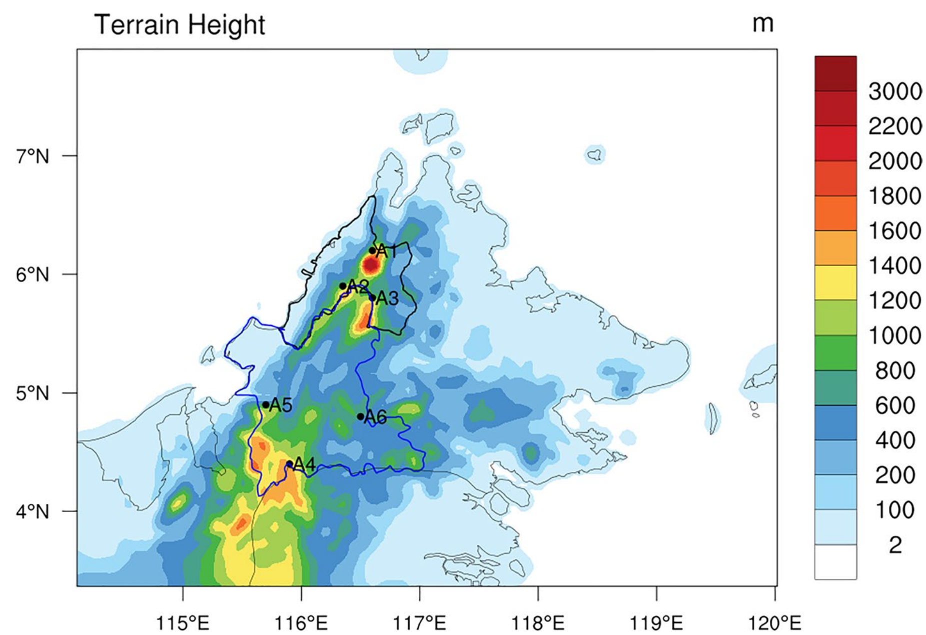

Fig. 10 Visualization of heavy rainfall locations, A1–A6, obtained from WRF E1 Domain 3. These locations are further categorized into the two regions represented by KK (black line—A1, A2, A3), and Keningau (blue—A4, A5, A6)

Table 7 Summary of heavy rainfall obtained from WRF model E1 Domain 3 from 16 to 18 Jul 2005

Area	Lat	Lon	Location	Total rainfall (mm)	No. of peaks	Hourly rainfall (max)		Basin	Catchment area (km^2)	Annual precipitation (mm)
						mm/h	UTC /date			
A1	6.11	116.54	Mount Kinabalu	201.31	8	32.75	0600 18 Jul	Kalimantan	881	3190
A2	5.85	116.35	Tuaran	149.15	3	36.10	0900 17 Jul	Kalimantan		
A3	5.80	116.60	Tambunan	128.66	5	26.44	1000 17 Jul	Padas	9726	2110
A4	4.40	115.90	Tenom	147.77	4	35.93	1200 17 Jul	Padas		
A5	4.90	115.70	Sipitang	153.67	5	31.26	1100 16 Jul	Padas		
A6	4.80	116.50	Sapulut	173.92	1	84.69	1200 16 Jul	Sapulut	5146	2491

at nearly the same time on 17 Jul. The simulated rainfall over the Kota Kinabalu region has the longest rainfall duration for 2 consecutive days. Therefore, the cause of the flash-flooding event from 17 to 19 Jul 2005 in the city was likely rooted to the prolonged heavy precipitation started since 0200 UTC 16 Jul and ended at 0600 UTC 18 Jul.

Finally, a total of 6 heavy rainfall locations were also identified using the simulated results from E1-D3 domain. They can be further categorized into two regions: KK and Keningau region. In the KK region, the locations are identified near to the Mount Kinabalu and in the Keningau region, the area is near to the Croker Range. The outcome of this study is important to provide early precaution and emphasis to the local authority and meteorological department in response to heavy rainfall event. We also found the cause of this severe flash flood is rooted to the prolonged heavy rainfall as explained above.

Sabah is well known as the “land below the wind”, because of its location at south of the typhoon-prone region, often making it insusceptible to the devastating effects of typhoons that frequently batter neighboring Philippines. Owing to this, the local authority often overlooked the possible impacts from tropical cyclone occurring in the mid-latitude. In addition, little attention has been paid to the threat of typhoons as the state priority from local research experts. In fact, our findings in this paper have revealed a close relationship between the tropical typhoon (Typhoon Haitang) and its possible association to heavy precipitation event occurred in Sabah. Such regional-to-local interaction between tropical cyclone occurred in South China Sea and air quality over Peninsula Malaysia is also reported in other study by Oozeer et al (2016). Though the typhoon did not direct hit on Sabah, the induced effect can be devastating to the city such that heavy precipitation prolonged over a long period of time. Particularly, the city Kota Kinabalu is one of the most populated areas in Sabah and is also the house to several tourism spots of the state. This is essential and important

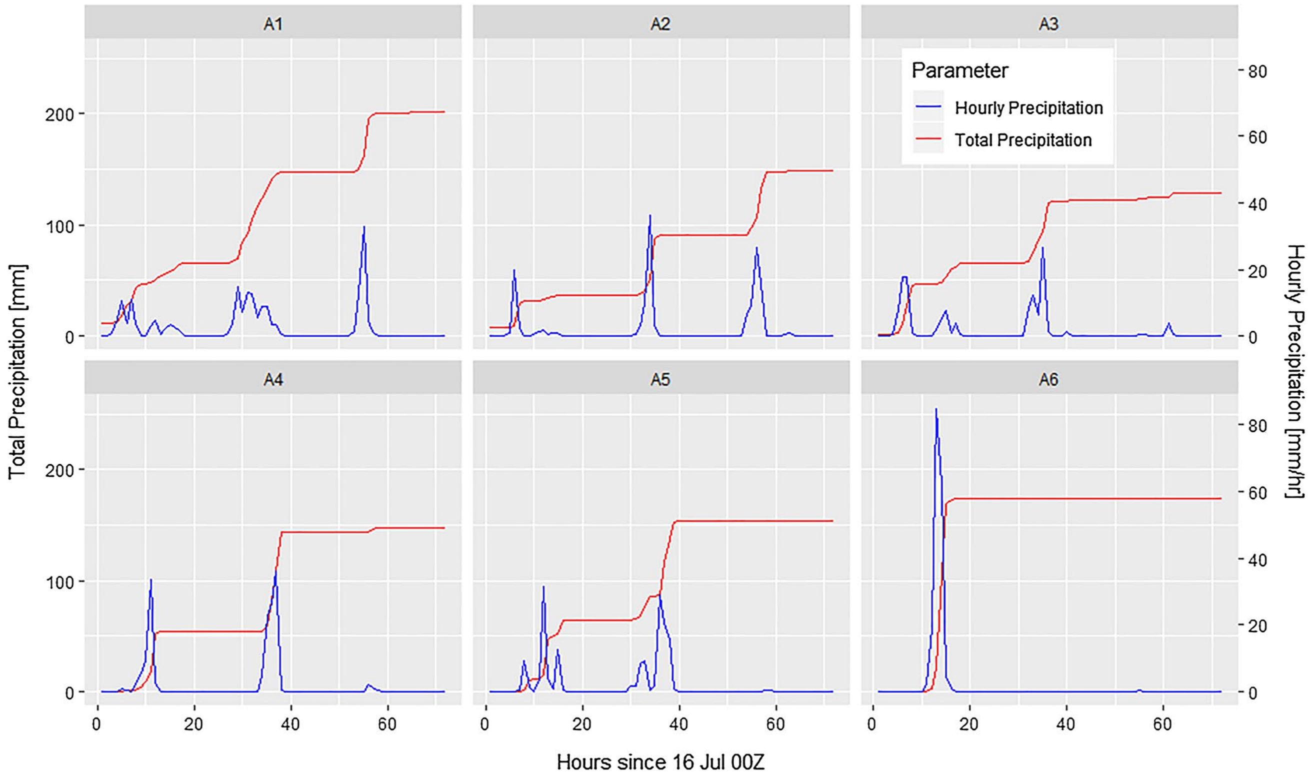

Fig. 11 The time evolution of total precipitation in mm and hourly precipitation in mm/h for the 6 heavy rainfall locations in Sabah region from 16 to 18 Jul. A1–A3 is located in Kota Kinabalu region, and A4–A6 is located in Keningau region

considering the most affected region has the highest population but the smallest water catchment. More work should be done in future to further investigate the occurrence of tropical cyclone under certain condition in terms of strength and distance from origin, which can possibly induce intensive precipitation over the region in Sabah.

Acknowledgements This research was supported by the Malaysian Ministry of Education under the research Grant number SBK0352-2017 and was greatly acknowledged.

References

Ardie WA, Sow KS, Tangang FT et al (2012) The performance of different cumulus parameterization schemes in simulating the 2006/2007 southern peninsular Malaysia heavy rainfall episodes. J Earth Syst Sci 121:317–327

Ashouri H, Gehne M, National Center for Atmospheric Research Staff (eds) (2018) Last modified 10 Dec 2018. The Climate Data Guide: PERSIANN-CDR: Precipitation Estimation from Remotely Sensed Information using Artificial Neural Networks—Climate Data Record. https://climatedataguide.ucar.edu/climate-data/persiann-cdr-precipitation-estimation-remotely-sensed-information-using-artificial.

Berrisford P, Dee D, Poli P, Brugge R, Fielding K, Fuentes M et al (2011) The ERA-Interim archive, version 2.0

Bruintjes RT, Clark TL, Hall WD (1994) Interactions between topographic airflow and cloud/precipitation development during the passage of a winter storm in Arizona. J Atmos Sci 51:48–67

Carbone RE, Tuttle JD, Ahijevych DA, Trier SB (2002) Inferences of predictability associated with warm season precipitation episodes. J Atmos Sci 59:2033–2056

Cardoso RM, Soares PMM, Miranda PMA, Belo-Pereira M (2013) WRF high resolution simulation of Iberian mean and extreme precipitation climate. Int J Climatol 33:2591–2608. https://doi.org/10.1002/joc.3616

Chawla I, Osuri KK, Mujumdar PP, Niyogi D (2018) Assessment of the weather research and forecasting (WRF) model for simulation of extreme rainfall events in the upper Ganga Basin. Hydrol Earth Syst Sci 22(2):5

Colle BA, Mass CF (1996) An observational and modeling study of the interaction of low-level southwesterly flow with the olympic mountains during COAST IOP 4. Mon Weather Rev 124:2152–2175. https://doi.org/10.1175/1520-0493(1996)124%3c2152:AOAMSO%3e2.0.CO;2

Colle BA, Mass CF, Westrick KJ (2000) MM5 precipitation verification over the Pacific Northwest during the 1997–99 cool seasons. Weather Forecast 15:730–744. https://doi.org/10.1175/1520-0434(2000)015%3c0730:MPVOTP%3e2.0.CO;2

Davis BAS, Brewer S, Stevenson AC, Guiot J (2003) The temperature of Europe during the Holocene reconstructed from pollen data. Q Sci Rev 22:1701–1716. https://doi.org/10.1016/S0277-3791(03)00173-2

Dee DP, Uppala SM, Simmons AJ, Berrisford P, Poli P, Kobayashi S et al (2011) The ERA-Interim reanalysis: configuration and performance of the data assimilation system. Q J R Meteorol Soc 137(656):553–597

Deng L, McCabe MF, Stenchikov G, Evans JP, Kucera PA (2015) Simulation of flash-flood-producing storm events in Saudi Arabia using the weather research and forecasting model. J Hydrometeorol 16(2):615–630
Dudhia J (1989) Numerical Study of convection observed during the winter monsoon experiment using a mesoscale two-dimensional model. J Atmos Sci 46:3077–3107. https://doi.org/10.1175/1520-0469(1989)046%3c3077:NSOCOD%3e2.0.CO;2
Efstathiou GA, Zoumakis NM, Melas D et al (2013) Sensitivity of WRF to boundary layer parameterizations in simulating a heavy rainfall event using different microphysical schemes: effect on large-scale processes. Atmos Res 132–133:125–143. https://doi.org/10.1016/j.atmosres.2013.05.004
Fiori E, Comellas A, Molini L, Rebora N, Siccardi F, Gochis DJ, Tanelli S, Parodi A (2014) Analysis and hindcast simulations of an extreme rainfall event in the Mediterranean area: the Genoa 2011 case. Atmos Res 138:13–29
Flesch TK, Reuter GW (2012) WRF model simulation of two Alberta flooding events and the impact of topography. J Hydrometeorol 13:695–708. https://doi.org/10.1175/JHM-D-11-035.1
Funk C, Peterson P, Landsfeld M, Pedreros D, Verdin J, Shukla S, Husak G, Rowland J, Harrison L, Hoell A, Michaelsen J (2015) The climate hazards infrared precipitation with stations—a new environmental record for monitoring extremes. Sci Data 2:150066
Gallus WAJ, Correia JJ, Jankov I (2005) The 4 June 1999 Derecho event: a particularly difficult challenge for numerical weather prediction. Weather Forecast 20:705–728. https://doi.org/10.1175/WAF883.1
Gaudet B, Cotton WR (1998) Statistical characteristics of a real-time precipitation forecasting model. Weather Forecast 13:966–982. https://doi.org/10.1175/1520-0434(1998)013%3c0966:SCOART%3e2.0.CO;2
Givati A, Lynn B, Liu Y, Rimmer A (2011) Using the WRF model in an operational streamflow forecast system for the Jordan River. J Appl Meteorol Climatol 51(2):285–299
Haghroosta T, Ismail WR, Ghafarian P, Barekati SM (2014) The efficiency of the Weather Research and Forecasting (WRF) model for simulating typhoons. Nat Hazards Earth Syst Sci 14:2179–2187. https://doi.org/10.5194/nhess-14-2179-2014
Hahn DC (2007) Evaluation of WRF performance for depicting orographically-induced gravity waves in the stratosphere. In: Proceedings of the 8th WRF user's workshop
Hong SY, Lee JW (2009) Assessment of the WRF model in reproducing a flash-flood heavy rainfall event over Korea. Atmos Res 93:818–831. https://doi.org/10.1016/j.atmosres.2009.03.015
Hong S, Lim J (2006) The WRF single-moment 6-class microphysics scheme (WSM6). J Korean Meteorol Soc 42:129–151
Hong S-Y, Dudhia J, Chen S-H (2004) A revised approach to ice microphysical processes for the bulk parameterization of clouds and precipitation. Mon Weather Rev 132:103–120. https://doi.org/10.1175/1520-0493(2004)132%3c0103:ARATIM%3e2.0.CO;2
Hong S-Y, Noh Y, Dudhia J (2006) A new vertical diffusion package with an explicit treatment of entrainment processes. Mon Weather Rev 134:2318–2341. https://doi.org/10.1175/MWR3199.1
Hong SY, Moon NK, Lim KS, Kim JW (2010) Future climate change scenarios over Korea using a multi-nested downscaling system: a pilot study. Asia Pac J Atmos Sci 46(4):425–435
Hsu KL, Gao X, Sorooshian S, Gupta HV (1997) Precipitation estimation from remotely sensed information using artificial neural networks. J App Meteor 36(9):1176–1190
Huffman GJ (1997) Estimates of root-mean-square random error for finite samples of estimated precipitation. J Appl Meteorol 36(9):1191–1201
Huffman GJ, Adler RF, Bolvin DT, Nelkin EJ (2010) The TRMM Multi-Satellite Precipitation Analysis (TMPA). Satellite rainfall applications for surface hydrology. Springer, Netherlands, Dordrecht, pp 3–22
Jee JB, Kim S (2017) Sensitivity study on high-resolution WRF precipitation forecast for a heavy rainfall event. Atmosphere 8(6):96
Kain JS (2004) The Kain–Fritsch convective parameterization: an update. J Appl Meteorol 43:170–181. https://doi.org/10.1175/1520-0450(2004)043%3c0170:TKCPAU%3e2.0.CO;2
Lee KO, Uyeda H, Lee DI (2014) Microphysical structures associated with enhancement of convective cells over Mt. Halla, Jeju Island, Korea on 6 Jul 2007. Atmos Res 135:76–90
Mass CF, Ovens D, Westrick K, Colle BA (2002) Does increasing horizontal resolution produce more skillful forecasts? Am Meteorol Soc 1:407–430. https://doi.org/10.1175/1520-0477(2002)083
Maussion F, Scherer D, Finkelnburg R, Richters J, Yang W, Yao T (2011) WRF simulation of a precipitation event over the Tibetan Plateau, China—an assessment using remote sensing and ground observations. Hydrol Earth Syst Sci 15(6):5
Mlawer EJ, Taubman SJ, Brown PD et al (1997) Radiative transfer for inhomogeneous atmospheres: RRTM, a validated correlated-k model for the longwave. J Geophys Res Atmos 102:16663–16682. https://doi.org/10.1029/97JD00237
Molg T, Chiang JCH, Gohm A, Cullen NJ (2009) Temporal precipitation variability versus altitude on a tropical high mountain: observations and mesoscale atmospheric modelling. Q J R Meteorol Soc 135:1439–1455
Oozeer MY, Chan A, Ooi MCG, Zarzur AM, Salinas SV, Chew BN, Morris KI, Choong WK (2016) Numerical study of the transport and convective mechanisms of biomass burning haze in South-Southeast Asia. Aerosol Air Qual Res 16:2950–2963
Parrish DF, Derber JC (1992) The National Meteorological Center's spectral statistical-interpolation analysis system. Mon Weather Rev 120(8):1747–1763
Rahmawati N, Lubczynski MW (2018) Validation of satellite daily rainfall estimates in complex terrain of Bali Island, Indonesia. Theor Appl Climatol 134:513–532
Raju PVS, Potty J, Mohanty UC (2011) Sensitivity of physical parameterizations on prediction of tropical cyclone Nargis over the Bay of Bengal using WRF model. Meteorol Atmos Phys 113:125–137. https://doi.org/10.1007/s00703-011-0151-y
Rogelis MC, Werner M (2018) Streamflow forecasts from WRF precipitation for flood early warning in mountain tropical areas. Hydrol Earth Syst Sci 22(1):853–870
Santos-Alamillos FJ, Pozo-Vázquez D, Ruiz-Arias JA, Lara-Fanego V, Tovar-Pescador J (2013) Analysis of WRF model wind estimate sensitivity to physics parameterization choice and terrain representation in Andalusia (Southern Spain). J Appl Meteorol Climatol 52(7):1592–1609
Singh J, Yeo K, Liu X et al (2015) Evaluation of WRF model seasonal forecasts for tropical region of Singapore. Adv Sci Res 12:69–72. https://doi.org/10.5194/asr-12-69-2015
Sorooshian S, Hsu K, Braithwaite D, Ashouri H (2014) NOAA climate data record (CDR) of precipitation estimation from remotely sensed information using artificial neural networks (PERSIANN-CDR), Version 1, Revision 1. https://gis.ncdc.noaa.gov/geoportal/catalog/search/resource/details.page
Weisman ML, Davis C, Wang W et al (2008) Experiences with 0–36-h explicit convective forecasts with the WRF-ARW model. Weather Forecast 23:407–437. https://doi.org/10.1175/2007WAF2007005.1
Wilson JW, Roberts RD (2006) Summary of convective storm initiation and evolution during IHOP: observational and modeling perspective. Mon Weather Rev 134:23–47. https://doi.org/10.1175/MWR3069.1
Xue M, Martin WJ (2006) A high-resolution modeling study of the 24 May 2002 dryline case during IHOP. Part I: Numerical simulation

and general evolution of the dryline and convection. Mon Weather Rev 134:149–171. https://doi.org/10.1175/MWR3071.1

Zhang D-L, Gao K, Parsons DB (1988) Numerical Simulation of an Intense Squall Line during 10–11 June 1985 PRE-STORM. Part I: model verification. Mon Weather Rev 117:960–994

Zhou J, Zhang H, Zhang J et al (2017) WRF model for precipitation simulation and its application in real-time flood forecasting in the Jinshajiang River Basin, China. Meteorol Atmos Phys 1:1–13. https://doi.org/10.1007/s00703-017-0542-9